

Lattice distortion induced first and second order topological phase transition in rectangular high- T_c superconducting monolayer

Li Chen,^{1,2,*} Bin Liu,^{1,2,*} Gang Xu,^{2,1,†} and Xin Liu^{1,2,‡}

¹*School of Physics, Huazhong University of Science and Technology, Wuhan, Hubei 430074, China*

²*Wuhan National High Magnetic Field Center, Huazhong University of Science and Technology, Wuhan, Hubei 430074, China*

(Dated: August 24, 2021)

We theoretically study the lattice distortion induced first and second order topological phase transition in rectangular $\text{FeSe}_x\text{Te}_{1-x}$ monolayer. When compressing the lattice constant in one direction, our first principles calculation shows that the $\text{FeSe}_x\text{Te}_{1-x}$ undergoes a band inversion at Γ point in a wide doping range, say $x \in (0.0, 0.7)$, which ensures coexistence of the topological band state and the high- T_c superconductivity. This unidirectional pressure also leads to the C_4 symmetry breaking which is necessary for the monolayer $\text{FeSe}_x\text{Te}_{1-x}$ to support Majorana corner states in the either presence or absence of time-reversal symmetry. Particularly, we use $k \cdot p$ methods to fit the band structure from the first principles calculation and found that the edge states along the (100) and (010) directions have different Dirac energy due to C_4 symmetry breaking. This is essential to obtain Majorana corner states in D class without concerning the details of the superconducting pairing symmetries and Zeeman form, which can potentially bring advantages in the experimental implementation.

PACS numbers: 74.45.+c, 75.70.Tj, 85.25.Cp

Introduction: The hybrid of superconductivity and topological band structure can provide an experimentally accessible platform to achieve the Majorana zero modes (MZMs) [1]. In the early studies, this hybrid is realized in the superconductor/topological insulator heterostructure through the superconducting proximity effect. The proximity induced superconducting gap is sensitive to the interface of the heterostructure and normally one order of magnitude smaller than the gap in the mother superconductor, which bring various difficulties in experimental verification of MZMs. Thus, it is essential to realize the MZMs in a large gap superconductor without complex heterostructure. On the other hand, iron-based superconductor was originally discovered as the first fully gapped high- T_c superconductors, which has multi-bands at the Fermi level [2–8]. Recent studies show that the existence of multi-bands at the Fermi level is helpful for the coexistence of high T_c superconductivity and topological band structure in one material without the complex heterostructure[9–12]. For instance, the zero bias conductance peak is observed at the surface vertex core [10, 13–15], following the theoretical prediction [16, 17]. Meanwhile, the theoretical studies of high order topological superconductors [18–39] provide the new insight to realize the MZM directly from two dimensional and three dimensional systems without breaking the uniformity of the bulk Hamiltonian. Thus, the implementation of the high order topological superconductors in iron-based superconductors can provide a promising approach to achieve the MZMs in one large gap superconductor and avoiding complex heterostructure.

In this work, we theoretically propose to realize the second order topological superconductor and MZMs in the monolayer rectangular $\text{FeSe}_x\text{Te}_{1-x}/\text{SrTiO}_3(110)$. First

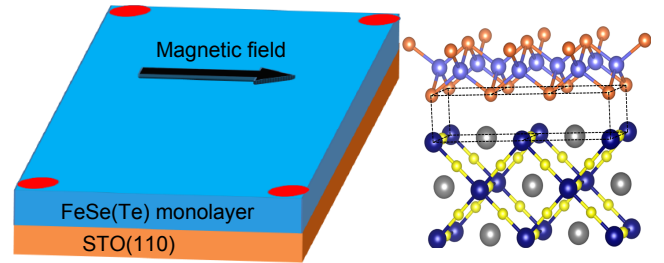


FIG. 1. Experimental set up of $\text{FeSe}_x\text{Te}_{1-x}/\text{SrTiO}_3(110)$ monolayer. The red points indicate the existence of Majorana corner states.

principles calculations show that the electronic band structure of the monolayer $\text{FeSe}_x\text{Te}_{1-x}$ can be driven from the trivial phase to strong TI phase when one of the in-plane lattice constant is reduced and system symmetry is broken down to D_{2h} in a wide range of composition x . This leads to the first order topological phase transition (TPT) of the inverted band structures in the AII class with one pair of helical edge states at each edge. To further considering the topological property in the presence of the superconductivity, we construct the electronic tight-binding model Hamiltonian based on the $k \cdot p$ method with realistic parameters through fitting the bands calculated from the first principles calculations. We note that the C_4 symmetry breaking is also necessary for the implementation of Majorana corner states in both time-reversal invariant and breaking monolayer $\text{FeSe}_x\text{Te}_{1-x}$. In particular, the edge states along (100) and (010) direction have different electronic Dirac energies, which naturally lead the two edges to be in different gapped phases in the presence of superconductivity and

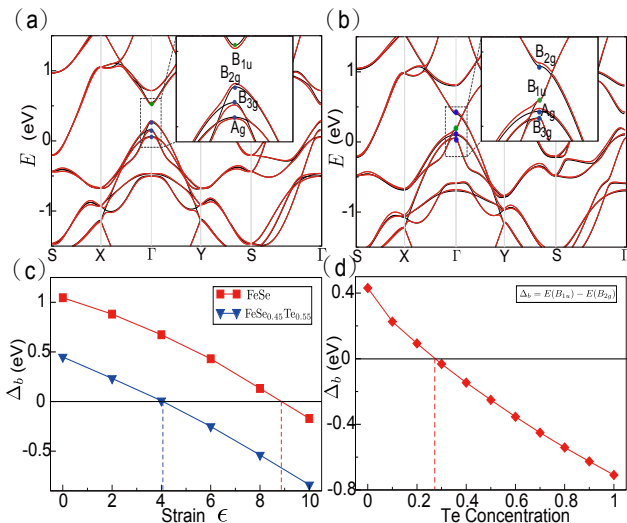


FIG. 2. (a) Band structure of $\text{FeSe}_{0.45}\text{Te}_{0.55}$ with the lattice distortion $\epsilon = 2\%$. (b) Band structure of $\text{FeSe}_{0.45}\text{Te}_{0.55}$ with the lattice distortion $\epsilon = 6\%$. (c) The band gap Δ_b of $\text{FeSe}_x\text{Te}_{1-x}$ monolayer as a function of distortion r with $x = 1$ (red lines) and $x = 0.45$ (blue lines). (d) The band gap Δ_b of $\text{FeSe}_x\text{Te}_{1-x}$ monolayer as a function of Te concentration $1 - x$ with $\epsilon = 6\%$.

in-plane magnetic field. Our results for D class monolayer rectangular $\text{FeSe}_x\text{Te}_{1-x}/\text{SrTiO}_3$ do not depend on the exact superconducting pairing symmetries (s wave pairing, s_{\pm} pairing) and the details of the Zeeman form, and are robust against disorders, which lead the rectangle monolayer $\text{FeSe}_x\text{Te}_{1-x}/\text{SrTiO}_3$ to be a promise candidate to realize MZMs without complex hybrid structures.

Lattice distortion induced First order TPT: The first principles calculations based on density functional theory (DFT) are carried out to study the topological property of the monolayer $\text{FeSe}_x\text{Te}_{1-x}$ with C_4 symmetry breaking. For the experimental reality, the system initially has square lattice with lattice constant $a_0 = 3.905\text{\AA}$, which is the same with the (001) monolayer $\text{FeSe}_x\text{Te}_{1-x}/\text{SrTiO}_3$ [12]. Without losing the generality, we consider to compress the lattice constant in [100] direction, quantified by the ration $\epsilon = (a_0 - a_x)/a_0$ with a_x the lattice constant along x direction after compression. The states at the Γ point are thus classified as the D_{2h} representations. Near Fermi level, we consider four orbital states, the odd parity states B_{1u} contributed by Se(Te) p_z orbital and the even parity states A_g , B_{2g} and B_{3g} mainly coming from Fe $d_{x^2-y^2}$, d_{xz} and d_{yz} orbitals respectively. We distinguish the parities by green and blue dots in Fig. 2(a). Note that the d_{xz} and d_{yz} orbitals are not degenerate any more due to the C_4 symmetry breaking. We first choose the typical composition value $x = 0.45$ [10] for which the monolayer $\text{FeSe}_x\text{Te}_{1-x}/\text{SrTiO}_3$ with C_4 symmetry is in topological trivial phase [12]. The calculated band structures for $\epsilon = 2\%$ and $\epsilon = 6\%$ are plotted in Fig. 2(a) and (b) re-

spectively, in which red and black curves correspond to the results calculated with spin-orbital coupling (SOC) and without SOC. For the bands of $\epsilon = 2\%$ shown in Fig. 2(a), there is no band inversion so that the system is still in topological trivial phase and has a positive band gap at Γ point $\Delta_b = E(B_{1u}) - E(B_{2g}) > 0$. For the bands of $\epsilon = 6\%$ shown in Fig. 2(b), band inversion happens between the odd parity state B_{1u} and even parity state B_{2g} at Γ point, and has a negative $\Delta_b < 0$. When SOC is excluded (see the black bands in Fig. 2b), there is a linear band crossing along $\Gamma - Y$ which is absent along $\Gamma - X$ due to the C_4 symmetry breaking. When SOC is included, a gap about 25 meV opens at the band crossing so that the system falls into a 2DTI phase around Γ point. Thus, the anisotropic lattice distortion, by increasing the compress ratio, induces the first order TPT. In Fig. 2(c), we plot the band gap Δ_b as a function of the compress ratio ϵ increasing from 0 to 10%, for different compositions $x = 0$ (red square for FeSe) and $x = 0.45$ (blue triangle for $\text{FeSe}_{0.55}\text{Te}_{0.45}$), respectively. The calculated results show that, both systems are initially in the trivial phase without compression ($\epsilon = 0$) [12] and the band gap Δ_b undergoes a sign change at the critical value $\epsilon_c = 9\%$ and $\epsilon_c = 4\%$ (indicated by red and blue dashed lines in Fig. 2(c)), for FeSe and $\text{FeSe}_{0.55}\text{Te}_{0.45}$ respectively. As reported by Ref. 40, high- T_c superconductivity has already been observed in $\text{FeSe}/\text{SrTiO}_3(110)$ with the rectangular lattice [40]. The $\text{SrTiO}_3(110)$ has the lattice constants $a = 3.905\text{\AA}$ and $b = \sqrt{2}a$. This lattice mismatch makes three unit cells of FeSe grow on the top of two $\text{STO}(110)$ unit cells, which reduces the FeSe lattice constant in [100] direction to $\frac{2}{3}\sqrt{2}a \approx 0.94a$, corresponding to $\epsilon = 6\%$ in our calculations. This growth technique should also be applied to $\text{FeSe}_x\text{Te}_{1-x}$ monolayer. We thus take $\epsilon = 6\%$ for the experimental reality and plot the band gap Δ_b as a function of the Te composition in Fig. 2(d). Such results strongly suggest that both the superconductivity and topological band structures could coexist in the rectangular lattice $\text{FeSe}_x\text{Te}_{1-x}$ for $0.3 < x < 0.7$ [12, 40, 41].

Model Hamiltonian: To further investigate the topological edge states, we construct an eight bands $k \cdot p$ effective model Hamiltonian with D_{2h} symmetry [42]. The full Hamiltonian with SOC in the basis $(|\uparrow\rangle, |\downarrow\rangle) \otimes (|yz\rangle, |x^2 - y^2\rangle, |xz\rangle, |z\rangle)$ takes the form $H(\mathbf{k}) = H_0 \otimes \mathbf{1}_2 + H_{soc}$ and the four bands model H_0 without SOC has the form:

$$H_0 = \begin{pmatrix} M_1(\mathbf{k}) & 0 & \beta k_x k_y & i\gamma k_y \\ 0 & M_2(\mathbf{k}) & 0 & 0 \\ \beta k_x k_y & 0 & M_3(\mathbf{k}) & i\delta k_x \\ -i\gamma k_y & 0 & -i\delta k_x & M_4(\mathbf{k}) \end{pmatrix}, \quad (1)$$

where $M_i(k) = E_i + M_{ix}k_x^2 + M_{iy}k_y^2$ ($i = 1, 2, 3, 4$). The C_4 symmetry breaking makes $M_{ix} \neq M_{iy}$. The parameters of our Hamiltonian are obtained by fitting the bands of the rectangle $\text{FeSe}_{0.45}\text{Te}_{0.55}$ (Fig. 2(b)). In Fig. 3(a), we show that, with the fitting parameters, our

model can describe the band dispersion near Γ point well. The explicit form of the Hamiltonian and fitting parameters can be found in Supplementary Materials [42]. With these parameters, in Fig. 3(b) we plot the band dispersions for the system in the slab geometry with the open boundary along x (black curves) and y (red curves) respectively. The Dirac points of these two edges have different energies with $E_u = 0.36$ eV (upper Dirac point) and $E_l = 0.31$ eV (lower Dirac point). The Dirac energy difference, δE_D is about 45 meV which is an order of magnitude larger than the superconducting gap and Zeeman splitting energy and consistent with the first principles calculations [42]. It is convenient to consider the system in Nambu space for including the superconductivity in mean field level. In this case, each edge has two Dirac points near the Fermi level because the degree of freedoms of the system is doubled. Note that as C_4 symmetry is broken by lattice distortion, the edge states should be considered separately for x and y edge. For simplicity, we first consider the chemical potential $\mu = E_u$, say at the Dirac point of the x edge (black curves in Fig. 3(b)). When the superconducting gap is absent, this Dirac point is doubled at $k_x = 0$ and the edge states are four fold degenerate which is protected by both time-reversal and charge U(1) symmetry. Along y direction (red curves in Fig. 3(b)), the electronic Dirac point at E_l is far below the chemical potential so that near the Fermi level there are two separated Dirac points, each of which is two fold degenerate and protected solely by the charge U(1) symmetry [42].

MZMs in DIII class: The pairing symmetry of the monolayer FeSe still has many debates in various studies which give plain s-wave pairing [43–47], s_{\pm} -wave pairing [48–52] and d-wave pairing [53–57]. Recent studies show that when the TI breaks C_4 symmetry, both s_{\pm} -wave pairing and d-wave pairing can lead to a pair of MZMs at each corner while plain s-wave pairing cannot [32, 34]. Here, we do not intend to distinguish these pairing symmetries but show that the rectangular monolayer $\text{FeSe}_x\text{Te}_{1-x}$ can potentially be high order time-reversal invariant TSC if it has s_{\pm} -wave or d-wave pairings. When applying the s_{\pm} -wave pairings $\Delta_{s0} - \Delta_{s1}(\cos(kx) + \cos(ky))$, the charge U(1) symmetries are broken so that the degeneracy at the Dirac points along x and y edges are lifted, which results in two gaps Δ_0^x and Δ_0^y (Fig. 3(c)). The gaps at x and y edges can change sign with varying the gap amplitude Δ_{s1} for given Δ_{s0} , leading to $\Delta_0^x \Delta_0^y < 0$ only in regime II (Fig. 3(d)) due to C_4 symmetry breaking, which is consistent with the results of Ref. 34. We calculate the eigenvalues of the system and found that a pair of MZMs at each corner appear in the regime of $\Delta_0^x \Delta_0^y < 0$ (Fig. 3(f)). The topological regime is roughly within 0.5 meV around $\Delta_{s0} = 2\Delta_{s1}$ for s_{\pm} pairing symmetry according to our fitting parameters.

MZMs in D class: When applying a magnetic field in-

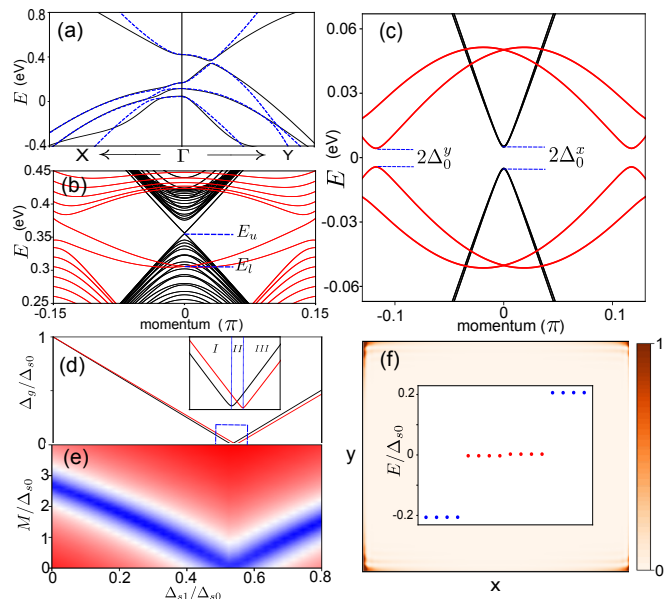


FIG. 3. (a) fitting the band dispersions (black) for $\epsilon = 6\%$ with $k \cdot p$ method (blue dash). (b) black and red curves for the band dispersions of k_x and k_y based on the fitting parameters in a slab geometry; (c) Band dispersions along x (black) and y (red) in Nambu space; (d) superconducting gap amplitudes at x (black) and y (red) edge as a function of Δ_{s1} without Zeeman field. (e) the gap amplitude at x edge as a function of Δ_{s1} and M (f) The density plot of the MZMs with TR symmetry. The inset plot the several lowest eigenenergies.

duced Zeeman term $M s_x$, the time-reversal symmetry is broken and the gaps for x and y edges behave in very different manners. Along x direction (Fig. 4(a)), both time-reversal and charge U(1) symmetries breaking results in two gap amplitudes $\Delta_{1(2)}^x = \Delta_0^x \pm \tilde{M}$ with \tilde{M} the Zeeman splitting of edge states [42]. As the superconducting gap and the Zeeman term commute, the states at the Dirac points are also the eigenstates of the superconducting matrix $\tau_x s_0$. The state with eigenenergy $-|\Delta_0^x - \tilde{M}|$ has the eigenvalue $\nu_2^x = -1(1)$ for $\Delta_0^x - \tilde{M} > (<)0$ respectively while the state with eigenenergy $-|\Delta_0^x + \tilde{M}|$ always has the eigenvalue $\nu_1^x = -1$. Along y direction (Fig. 4(a)), the gap amplitudes are almost independent of the Zeeman term and have $\Delta_1^y = \Delta_2^y \approx \Delta_0^y$ for $\tilde{M} \ll \delta E_D$ [42]. We thus can define a Z_2 topological invariant $(-1)^\nu = \text{sign}(\nu_1^x \nu_2^x)$. Based on our model Hamiltonian, the eigenvalues of the system are calculated for both $\nu = 0, 1$. We found that there are four states with zero eigenvalues, which are MZMs and localized at the four corners for $\nu = 1$ (Fig. 4(b)) while the MZMs are absent for $\nu = 0$. In Fig. 3(e), we show that to achieve $\nu = 1$ has no limit to the ratio Δ_{s1}/Δ_{s0} . This means the implementation of Majorana corner state in D class monolayer $\text{FeSe}_x\text{Te}_{1-x}$ is not sensitive to the superconducting pairing symmetries. Without loss of generality, we take $\Delta_{s1} = 0$ in the rest of this work. So far the

chemical potential is taken $\mu = E_u$. When we vary the chemical potential, the Majorana corner states still exist in a wide chemical potential range. We calculate the lowest eigenenergy of the closed system as function of chemical potential and magnetic field. The color plot of the eigenenergy (Fig. 4(c)) shows an obvious phase boundary between zero (blue) and finite (red) values. We also calculate the critical magnetic field (black curve in Fig. 4(c)), where the gap of the edge state along x direction is closed, as a function of chemical potential. The phase boundary matches the critical magnetic field well, which means the Majorana corner states in our work is not sensitive to the chemical potential as long as it does not close the edge states gap.

As the anisotropic edge states, resulting in the different electronic Dirac point energies, is essential for realize the Majorana corner state, we construct the edge theory to study the effect of the lattice distortion on the edge states. Because the band inversion at Γ point only take place between $|xz\rangle$ and $|z\rangle$ orbitals with the highest two energies, without loss of generality, we can construct our edge theory in a simplified model [34]

$$H_{eff}(k) = B(k)s_0\sigma_z - D(k)s_0\sigma_0 - \eta k_x s_0\sigma_y + \alpha k_y s_z\sigma_x,$$

by projecting the Hamiltonian (Eq. (1)) into these two orbitals with $D(k) = D_x k_x^2 + D_y k_y^2$ and $B(k) = E_b - B_x k_x^2 - B_y k_y^2$. Note that the term with $D(k)$ breaks the conduction-valence symmetry of the bands while $D_x \neq D_y$ and $B_x \neq B_y$ due to the C_4 symmetry breaking.

At first we consider the edge states in (100) direction for the semi-infinite system with $y \in (0, \infty)$. In this case, we decompose the Hamiltonian as $H_{eff} = H_0 + H_p$ with

$$\begin{aligned} H_0(k_x, -i\partial_y) &= (E_b + B_y \partial_y^2) s_0 \sigma_z - i\alpha \partial_y s_z \sigma_x, \\ H_p(k_x, -i\partial_y) &= D_y \partial_y^2 s_0 \sigma_0 - \eta k_x s_0 \sigma_y. \end{aligned} \quad (2)$$

By projecting the Hamiltonian H_p into the basis $\psi_{\alpha=1,2}(y)$, which are the eigenstates of H_0 , we obtain the effective edge states Hamiltonian

$$H_x(k_x) = \frac{D_y E_b}{B_y} \tilde{s}_0 + \eta k_x \tilde{s}_z \quad (3)$$

with \tilde{s} the Pauli matrix acting in edge states space. Similar we can also obtain the edge states Hamiltonian in (010) direction which has the form

$$H_y(k_y) = \frac{D_x E_b}{B_x} \tilde{s}_0 - \alpha k_y \tilde{s}_z. \quad (4)$$

We found that the difference of the Dirac energies $E_u - E_l = E_b(\frac{D_y}{B_y} - \frac{D_x}{B_x})$ which is only finite with breaking both conduction-valence band symmetry ($D_i \neq 0$) and C_4 symmetry ($B_x \neq B_y$) spontaneously. The former is naturally satisfied for $|z\rangle$ and $|xz\rangle$ orbitals. With the fitting parameters, we find that $E_u - E_l = 48$ meV calculated from the four band model is consistent with DFT calculations[42].

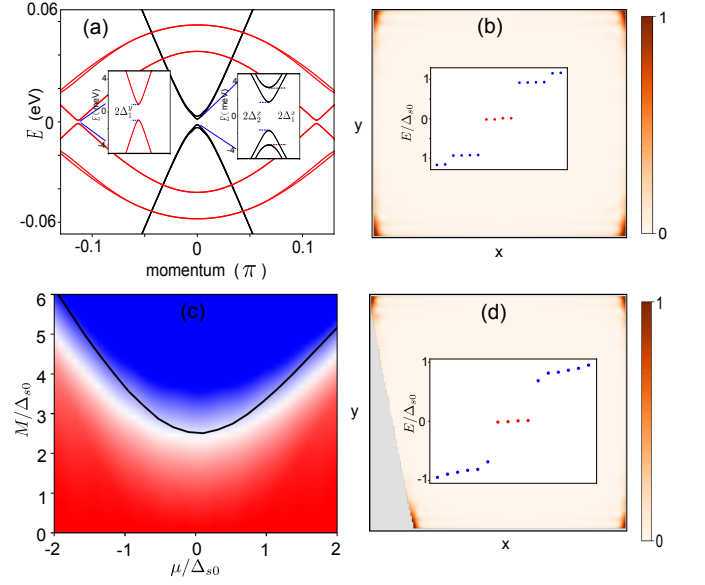


FIG. 4. (a) Band dispersions along x (black) and y (red) in Nambu space with magnetic field. (b) The density plot of the MZMs with magnetic field which break TR symmetry. The inset plot the several lowest eigenenergies. (c) Phase diagram with chemical potential and magnetic field. (d) The density distribution and energies of MZMs when the shape of corner is not perfect.

Discussion and conclusion: Considering the experimental reality, the d-orbitals of the iron-based superconductors may have very complicated g factor, which can result in orbital dependent Zeeman term other than $M\sigma_0 s_x$. However, the various Zeeman terms can always lead to the transition from $\nu = 0$ to $\nu = 1$ [42]. Thus our results are independent of the special Zeeman forms. The edges of the iron-based superconductor may not be perfectly along x or y directions and the corner maybe not sharp, which however do not affect the robustness of the Majorana corner state due to its protection only from particle-hole symmetry. In Fig. 4(d), the four eigenfunctions with the lowest eigenvalues are plotted in the system whose two neighbor edges have a angle 105° with smooth corners. These states localize at the four corners with perfect zero energy which shows the robustness of the MZMs under the imperfect edges and corners. In conclusion, the C_4 symmetry breaking by the lattice distortion in monolayer $\text{FeSe}_x\text{Te}_{1-x}$ can lead to the first order topological phase transition in the wide composition range $x \in (0, 0.7)$, which includes the regime for the monolayer $\text{FeSe}_x\text{Te}_{1-x}$ with the critical temperature up to 65K [41]. This rectangular monolayer $\text{FeSe}_x\text{Te}_{1-x}$ is also a promise candidate to realize Majorana corner states.

ACKNOWLEDGEMENT

We would like to thank Chao-Xing Liu, Chen Fang, Ling-Yuan Kong and Yi Zhou for fruitful discussions. G. Xu acknowledges the support of the Ministry of Science and Technology of China (Grant No. 2018YFA0307000), and the NFSC (Grant No. 11874022). X. Liu acknowledges the support of National Key R&D Program of China (Grant No. 2016YFA0401003) and NSFC (Grant No. 11674114).

* These authors contribute equally to this work.

† gangxu@hust.edu.cn

‡ phyliuxin@hust.edu.cn

- [1] L. Fu and C. L. Kane, *Phys. Rev. Lett.* **100**, 096407 (2008).
- [2] T. Hanaguri, S. Niitaka, K. Kuroki, and H. Takagi, *Science* **328**, 474 (2010), <https://science.sciencemag.org/content/328/5977/474.full.pdf>.
- [3] F. Li, H. Ding, C. Tang, J. Peng, Q. Zhang, W. Zhang, G. Zhou, D. Zhang, C.-L. Song, K. He, S. Ji, X. Chen, L. Gu, L. Wang, X.-C. Ma, and Q.-K. Xue, *Phys. Rev. B* **91**, 220503 (2015).
- [4] J.-F. Ge, Z.-L. Liu, C. Liu, C.-L. Gao, D. Qian, Q.-K. Xue, Y. Liu, and J.-F. Jia, *Nature Materials* **14**, 285 (2014).
- [5] Q.-Y. Wang, Z. Li, W.-H. Zhang, Z.-C. Zhang, J.-S. Zhang, W. Li, H. Ding, Y.-B. Ou, P. Deng, K. Chang, J. Wen, C.-L. Song, K. He, J.-F. Jia, S.-H. Ji, Y.-Y. Wang, L.-L. Wang, X. Chen, X.-C. Ma, and Q.-K. Xue, *Chinese Physics Letters* **29**, 037402 (2012).
- [6] C.-L. Song, Y.-L. Wang, P. Cheng, Y.-P. Jiang, W. Li, T. Zhang, Z. Li, K. He, L. Wang, J.-F. Jia, H.-H. Hung, C. Wu, X. Ma, X. Chen, and Q.-K. Xue, *Science* **332**, 1410 (2011), <https://science.sciencemag.org/content/332/6036/1410.full.pdf>.
- [7] F.-C. Hsu, J.-Y. Luo, K.-W. Yeh, T.-K. Chen, T.-W. Huang, P. M. Wu, Y.-C. Lee, Y.-L. Huang, Y.-Y. Chu, D.-C. Yan, and M.-K. Wu, *Proceedings of the National Academy of Sciences* **105**, 14262 (2008), <https://www.pnas.org/content/105/38/14262.full.pdf>.
- [8] Z. Wang, P. Zhang, G. Xu, L. K. Zeng, H. Miao, X. Xu, T. Qian, H. Weng, P. Richard, A. V. Fedorov, H. Ding, X. Dai, and Z. Fang, *Phys. Rev. B* **92**, 115119 (2015).
- [9] P. Zhang, Z. Wang, X. Wu, K. Yaji, Y. Ishida, Y. Kohama, G. Dai, Y. Sun, C. Bareille, K. Kuroda, T. Kondo, K. Okazaki, K. Kindo, X. Wang, C. Jin, J. Hu, R. Thomale, K. Sumida, S. Wu, K. Miyamoto, T. Okuda, H. Ding, G. D. Gu, T. Tamegai, T. Kawakami, M. Sato, and S. Shin, *Nature Physics* **15**, 41 (2019).
- [10] P. Zhang, K. Yaji, T. Hashimoto, Y. Ota, T. Kondo, K. Okazaki, Z. Wang, J. Wen, G. D. Gu, H. Ding, and S. Shin, *Science* **360**, 182 (2018), <https://science.sciencemag.org/content/360/6385/182.full.pdf>.
- [11] X. Wu, S. Qin, Y. Liang, H. Fan, and J. Hu, *Phys. Rev. B* **93**, 115129 (2016).
- [12] X. L. Peng, Y. Li, X. X. Wu, H. B. Deng, X. Shi, W. H. Fan, M. Li, Y. B. Huang, T. Qian, P. Richard, J. P. Hu, S. H. Pan, H. Q. Mao, Y. J. Sun, and H. Ding, arXiv e-prints , arXiv:1903.05968 (2019), [arXiv:1903.05968](https://arxiv.org/abs/1903.05968) [[arXiv:1903.05968](https://arxiv.org/archive/mat) [\[cond-mat.supr-con\]](https://arxiv.org/archive/mat)].
- [13] L. Kong, S. Zhu, M. Papaj, L. Cao, H. Isobe, W. Liu, D. Wang, P. Fan, H. Chen, Y. Sun, S. Du, J. Schneeloch, R. Zhong, G. Gu, L. Fu, H.-J. Gao, and H. Ding, arXiv e-prints , arXiv:1901.02293 (2019), [arXiv:1901.02293](https://arxiv.org/abs/1901.02293) [[arXiv:1901.02293](https://arxiv.org/archive/mat) [\[cond-mat.supr-con\]](https://arxiv.org/archive/mat)].
- [14] S. Zhu, L. Kong, L. Cao, H. Chen, S. Du, Y. Xing, W. Liu, D. Wang, C. Shen, F. Yang, J. Schneeloch, R. Zhong, G. Gu, L. Fu, Y.-Y. Zhang, H. Ding, and H.-J. Gao, arXiv e-prints , arXiv:1904.06124 (2019), [arXiv:1904.06124](https://arxiv.org/abs/1904.06124) [[arXiv:1904.06124](https://arxiv.org/archive/mat) [\[cond-mat.supr-con\]](https://arxiv.org/archive/mat)].
- [15] Q. Liu, C. Chen, T. Zhang, R. Peng, Y.-J. Yan, C.-H.-P. Wen, X. Lou, Y.-L. Huang, J.-P. Tian, X.-L. Dong, G.-W. Wang, W.-C. Bao, Q.-H. Wang, Z.-P. Yin, Z.-X. Zhao, and D.-L. Feng, *Phys. Rev. X* **8**, 041056 (2018).
- [16] G. Xu, B. Lian, P. Tang, X.-L. Qi, and S.-C. Zhang, *Phys. Rev. Lett.* **117**, 047001 (2016).
- [17] P. Hosur, P. Ghaemi, R. S. K. Mong, and A. Vishwanath, *Phys. Rev. Lett.* **107**, 097001 (2011).
- [18] F. Zhang, C. L. Kane, and E. J. Mele, *Phys. Rev. Lett.* **110**, 046404 (2013).
- [19] W. A. Benalcazar, B. A. Bernevig, and T. L. Hughes, *Phys. Rev. B* **96**, 245115 (2017).
- [20] J. Langbehn, Y. Peng, L. Trifunovic, F. von Oppen, and P. W. Brouwer, *Phys. Rev. Lett.* **119**, 246401 (2017).
- [21] Z. Song, Z. Fang, and C. Fang, *Phys. Rev. Lett.* **119**, 246402 (2017).
- [22] M. Ezawa, *Phys. Rev. Lett.* **120**, 026801 (2018).
- [23] H. Shapourian, Y. Wang, and S. Ryu, *Phys. Rev. B* **97**, 094508 (2018).
- [24] X. Zhu, *Phys. Rev. B* **97**, 205134 (2018).
- [25] M. Geier, L. Trifunovic, M. Hoskam, and P. W. Brouwer, *Phys. Rev. B* **97**, 205135 (2018).
- [26] E. Khalaf, *Phys. Rev. B* **97**, 205136 (2018).
- [27] F. Schindler, A. M. Cook, M. G. Vergniory, Z. Wang, S. S. P. Parkin, B. A. Bernevig, and T. Neupert, *Science Advances* **4** (2018), 10.1126/sciadv.aat0346, <https://advances.sciencemag.org/content/4/6/eaat0346.full.pdf>.
- [28] M. Ezawa, *Phys. Rev. B* **97**, 241402 (2018).
- [29] F. Schindler, Z. Wang, M. G. Vergniory, A. M. Cook, A. Murani, S. Sengupta, A. Y. Kasumov, R. Deblock, S. Jeon, I. Drozdov, H. Bouchiat, S. Guron, A. Yazdani, B. A. Bernevig, and T. Neupert, *Nat. Phys.* **14**, 918 (2018).
- [30] M. Ezawa, *Phys. Rev. B* **98**, 045125 (2018).
- [31] M. Ezawa, *Phys. Rev. B* **97**, 155305 (2018).
- [32] Q. Wang, C.-C. Liu, Y.-M. Lu, and F. Zhang, *Phys. Rev. Lett.* **121**, 186801 (2018).
- [33] V. Dwivedi, C. Hickey, T. Eschmann, and S. Trebst, *Phys. Rev. B* **98**, 054432 (2018).
- [34] Z. Yan, F. Song, and Z. Wang, *Phys. Rev. Lett.* **121**, 096803 (2018).
- [35] Y. Wang, M. Lin, and T. L. Hughes, *Phys. Rev. B* **98**, 165144 (2018).
- [36] C.-H. Hsu, P. Stano, J. Klinovaja, and D. Loss, *Phys. Rev. Lett.* **121**, 196801 (2018).
- [37] X.-H. Pan, K.-J. Yang, L. Chen, G. Xu, C.-X. Liu, and X. Liu, arXiv e-prints , arXiv:1812.10989 (2018), [arXiv:1812.10989](https://arxiv.org/abs/1812.10989) [[arXiv:1812.10989](https://arxiv.org/archive/mat) [\[cond-mat.mes-hall\]](https://arxiv.org/archive/mat)].
- [38] X. Wu, X. Liu, R. Thomale, and C.-X. Liu, arXiv e-prints , arXiv:1905.10648 (2019), [arXiv:1905.10648](https://arxiv.org/abs/1905.10648) [[arXiv:1905.10648](https://arxiv.org/archive/mat) [\[cond-mat.supr-con\]](https://arxiv.org/archive/mat)].

- [39] R.-X. Zhang, W. S. Cole, and S. Das Sarma, *Phys. Rev. Lett.* **122**, 187001 (2019).
- [40] P. Zhang, X.-L. Peng, T. Qian, P. Richard, X. Shi, J.-Z. Ma, B. B. Fu, Y.-L. Guo, Z. Q. Han, S. C. Wang, L. L. Wang, Q.-K. Xue, J. P. Hu, Y.-J. Sun, and H. Ding, *Phys. Rev. B* **94**, 104510 (2016).
- [41] X. Shi, Z.-Q. Han, P. Richard, X.-X. Wu, X.-L. Peng, T. Qian, S.-C. Wang, J.-P. Hu, Y.-J. Sun, and H. Ding, *Science Bulletin* **62**, 503 (2017).
- [42] See supplementary material.
- [43] D. Liu, W. Zhang, D. Mou, J. He, Y.-B. Ou, Q.-Y. Wang, Z. Li, L. Wang, L. Zhao, S. He, Y. Peng, X. Liu, C. Chen, L. Yu, G. Liu, X. Dong, J. Zhang, C. Chen, Z. Xu, J. Hu, X. Chen, X. Ma, Q. Xue, and X. J. Zhou, *Nature Communications* **3**, 931 (2012).
- [44] Q. Fan, W. H. Zhang, X. Liu, Y. J. Yan, M. Q. Ren, R. Peng, H. C. Xu, B. P. Xie, J. P. Hu, T. Zhang, and D. L. Feng, *Nature Physics* **11**, 946 (2015).
- [45] C. Fang, Y.-L. Wu, R. Thomale, B. A. Bernevig, and J. Hu, *Phys. Rev. X* **1**, 011009 (2011).
- [46] Y. Zhou, D.-H. Xu, F.-C. Zhang, and W.-Q. Chen, *EPL (Europhysics Letters)* **95**, 17003 (2011).
- [47] F. Yang, F. Wang, and D.-H. Lee, *Phys. Rev. B* **88**, 100504 (2013).
- [48] G. R. Stewart, *Rev. Mod. Phys.* **83**, 1589 (2011).
- [49] P. J. Hirschfeld, M. M. Korshunov, and I. I. Mazin, *Reports on Progress in Physics* **74**, 124508 (2011).
- [50] I. I. Mazin, *Phys. Rev. B* **84**, 024529 (2011).
- [51] Z. P. Yin, K. Haule, and G. Kotliar, *Nature Physics* **10**, 845 (2014).
- [52] J. Hu, *Phys. Rev. X* **3**, 031004 (2013).
- [53] Y. Zhang, J. J. Lee, R. G. Moore, W. Li, M. Yi, M. Hashimoto, D. H. Lu, T. P. Devereaux, D.-H. Lee, and Z.-X. Shen, *Phys. Rev. Lett.* **117**, 117001 (2016).
- [54] D. F. Agterberg, T. Shishidou, J. O'Halloran, P. M. R. Brydon, and M. Weinert, *Phys. Rev. Lett.* **119**, 267001 (2017).
- [55] Z. Ge, C. Yan, H. Zhang, D. Agterberg, M. Weinert, and L. Li, *Nano Lett.* **19**, 2497 (2019).
- [56] T. A. Maier, S. Graser, P. J. Hirschfeld, and D. J. Scalapino, *Phys. Rev. B* **83**, 100515 (2011).
- [57] F. Wang, F. Yang, M. Gao, Z.-Y. Lu, T. Xiang, and D.-H. Lee, *EPL (Europhysics Letters)* **93**, 57003 (2011).